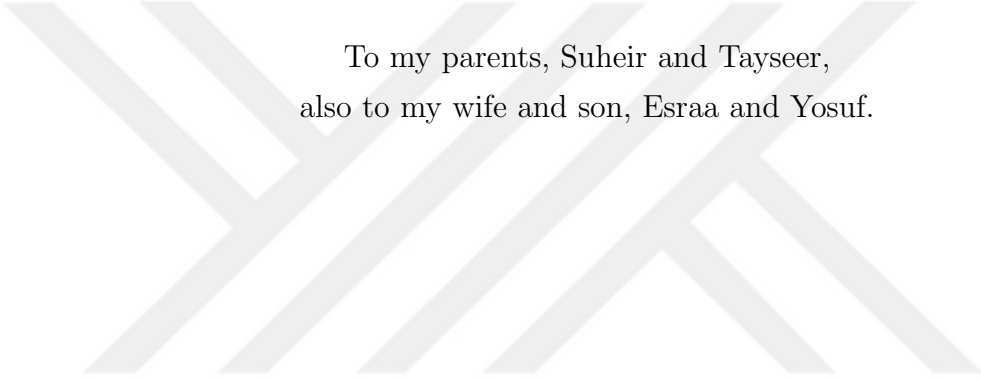


NOMA MULTI-NUMEROLOGY AND GUARD REDUCTION METHODS IN OFDM SYSTEMS FOR 5G NETWORKS

A THESIS SUBMITTED TO
THE GRADUATE SCHOOL OF
ENGINEERING AND NATURAL SCIENCES
OF ISTANBUL MEDIPOL UNIVERSITY
IN PARTIAL FULFILLMENT OF THE REQUIREMENTS FOR
THE DEGREE OF
MASTER OF SCIENCE
IN
ELECTRICAL, ELECTRONICS ENGINEERING AND CYBER SYSTEMS

By
Ayman Abu Sabah

June, 2018



To my parents, Suheir and Tayseer,
also to my wife and son, Esraa and Yosuf.

ABSTRACT

NOMA MULTI-NUMEROLOGY AND GUARD REDUCTION METHODS IN OFDM SYSTEMS FOR 5G NETWORKS

Ayman Abu Sabah

M.S. in Electrical, Electronics Engineering and Cyber Systems

Advisor: Prof. Dr. Hüseyin Arslan

June, 2018

Non-orthogonal multiple access (NOMA) is a promising technique which outperforms the traditional multiple access schemes in many aspects. It uses superposition coding (SC) to share the available resources among the users and adopts successive interference cancellation (SIC) for multiuser detection (MUD). Detection is performed in the power domain where fairness can be supported through appropriate power allocation. Since power domain NOMA utilizes SC at the transmitter and SIC at the receiver, users cannot achieve equal rates and experience higher interference. In this thesis, a novel NOMA scheme is proposed for multi-numerology (NR) orthogonal frequency division multiplexing (OFDM) system, i.e., different subcarrier spacings (SCSs). The scheme uses the nature of mixed NR systems to reduce the constraints associated with the MUD operation. This scheme not only enhances the fairness among the users but it improves the bit error rate performance as well. Although the proposed scheme is less spectrally efficient than conventional NOMA schemes, it is still more spectrally efficient than orthogonal multiple access schemes. As another contribution, we propose a novel frame structure for fifth generation (5G) networks. Such the structure aims to increase the capability of adopting the NR in 5G networks. In particular, a common cyclic prefix is appended to multiple OFDM symbols. Therefore, adopting large SCSs or short OFDM symbols becomes more flexible and applicable.

Keywords: Non-orthogonal multiple access (NOMA), fifth generation (5G), numerology (NR), orthogonal frequency division multiplexing (OFDM), fairness, 5G frame structure, cyclic prefix (CP) overhead, spectral efficiency.

ÖZET

5G AGLARINDA OFDM SİSTEMLERİ İÇİN NOMA ÇOKLU NUMEROLOJİSİ VE KORUMA BANDI AZALTIM YÖNTEMLERİ

Ayman Abu Sabah

Elektrik-Elektronik Mühendisliği ve Siber Sistemler, Yüksek Lisans

Tez Danışmanı: Prof. Dr. Hüseyin Arslan

Haziran, 2018

Dikgen olmayan çoklu erişim (NOMA) yöntemi, birçok yönden geleneksel çoklu erişim (MA) tekniklerini geride bırakan ve gelecekte kullanılması beklenen tekniklerden biridir. Kullanıma açık kaynakları kullanıcılar arasında paylaşmak için süper-pozisyon kodlaması (SC) kullanır ve çok kullanıcılı algılama (MUD) için ardışık girişim giderim (SIC) yöntemi kullanır. Sinyallerin tespiti ise adil olarak uygun güç tahsisi (PA) yöntemi ile güç uzayında gerçekleştirilir. NOMA güç alanı, alıcıda (RX) SC, vericide (TX) ise SIC kullanılması sebebiyle kullanıcılar eşit hızlara ulaşamaz ve daha yüksek bir girişim yaşayamaz. Bu tezde ise çoklu numeroloji (NR) dikgen frekans bölmeli çoğullama (OFDM) sistemi, yani farklı alt taşıyıcı aralıkları (SCS' ler) için yeni bir NOMA şeması önerilmiştir. Önerilen şema, MUD işlemiyle ilişkili kısıtlamaları azaltmak için karışık NR sistemlerinin doğal özelliklerini kullanır. Bu şema sadece kullanıcılar arasındaki adil uygulama oranını arttırmakla kalmaz, aynı zamanda bit hata oranı performansını da (BER) geliştirir. Önerilen plan geleneksel NOMA yöntemlerinden spektrum verimliliğinin açısından daha az olsa da Dikgen çoklu erişim (OMA) şemalarından spektrum verimliliği açısından daha zengindir. Bu olumlu yönlere ek başka bir katkı da OFDM sistemlerinde gereken koruma ekleri, örneğin döngüsel öneki (CP) azaltmak için yeni bir alıcı verici tasarımı önermekteyiz. Bir dizi OFDM sembolü TX' de bir CP' ye eklenir. RX' de, genişletilmiş hızlı bir Fourier dönüşümü (FFT) çalışması, uzunluğun CP ile çıkartılmış sinyale eşittir. Sonuç olarak, dikgen olarak iletilen semboller yapıcı bir eklenti olarak eklenir. Bu matematiksel olarak kanıtlanmıştır. Sonuç olarak, çoğullanmış sembolleri ayırmak için iki yaklaşım benimsenmiştir.

Anahtar sözcükler: Dikgen olmayan çoklu giriş (NOMA), dikgen frekans bölmeli

çoğullama (OFDM), çoklu numeroloji (NR), bit hata oranı (BER), uygunluk, koruma azaltma, döngüsel önek (CP), yüksek güvenilirlikli ve az gecikmeli haberleşme (URLLC), spektral verimlilik (SE).



Acknowledgement

Foremost, I want to offer this endeavor to our God Almighty for the wisdom he has bestowed upon me, the strength, peace of mind and good health in order to finish this research.

I would like to express my sincere gratitude to my advisor, Prof. Dr. Hüseyin Arslan for the continuous support of my Master studies and research, for his patience, motivation, enthusiasm, and immense knowledge. His guidance helped me in all the time of research and writing of this thesis. My sincere thanks also go to my wife Mrs. Esraa Jaradat for her sincere support and contribution throughout the conduction of this research work. Special thanks to my colleagues at CoSiNC research group for the encouragement and advise we share in pursuing and achieving our research goals.

My heartfelt thanks and appreciation goes to my beloved parents: Suheir and Tayseer, for giving birth to me at first place and for supporting and shaping me to the individual I am today. May the blessing be showered on them as they have done to me since I was young. Last but not the least, my honest and sincere words to my wife and my lovely son: I love all of you.

Contents

1	Introduction	1
2	NOMA Multi-Numerology OFDM Systems for 5G Networks	2
2.1	Orthogonal Multiple Access	2
2.2	Conventional Power-Domain NOMA	3
2.3	Main Advantages of NOMA	4
2.4	Numerology Concept	5
2.5	Problem Description	5
2.6	Proposed Solution	6
2.7	Signal Configuration	8
2.8	Conventional NOMA Versus Proposed NOMA	10
2.8.1	Conventional NOMA (CN)	11
2.8.2	Proposed NOMA (PN)	11
2.9	Conventional NOMA System Model	12

2.10	Proposed NOMA Design Analysis	13
2.11	Performance Evaluation	17
2.11.1	BER	17
2.11.2	Fairness Factor (F)	18
2.11.3	Spectral Efficiency (SE)	20
2.12	Conclusion	21
3	Common Cyclic Prefix for Numerology-5G Frame Structure	23
3.1	Numerology for 5G Frame Structure	23
3.2	Problem Description	24
3.3	State of Art	25
3.4	Proposed Solution	25
3.5	Design Analysis	26
3.6	Detection Approaches	29
3.6.1	First Approach	29
3.6.2	Second Approach	30
3.7	Performance Evaluation	31
3.8	Conclusion	34
4	Future Work	35

5 Appendix 37

5.1 Appendix A: Detailed Derivations of Mathematical Equations . . . 37



List of Figures

2.1	Orthogonal multiple access techniques.	3
2.2	Power-domain NOMA.	4
2.3	Signals superposition in time and frequency domains.	7
2.4	Two different user distribution scenarios.	10
2.5	Transceiver design for proposed NOMA scheme adopting three downlink users.	17
2.6	BER performance utilizing conventional and proposed NOMA. . .	19
2.7	Fairness level of conventional and proposed NOMA utilizing the optimum PA for the second scenario.	20
2.8	Average SE adopting conventional NOMA, proposed NOMA and OMA using the optimum PA for the first scenario.	21
3.1	5G-NR frame structure.	24
3.2	Transmitter design where $Q = 2$	27
3.3	Receiver design adopting the first approach where $Q = 2$	29

3.4 Receiver design adopting the second approach where $Q = 2$ 32

3.5 The SE performance over multipath channel, SCS = 15kHz. . . . 33

3.6 The SER performance over multipath channel where the normalized CFO = .03. 34



List of Tables

2.1	Simulation Parameters.	16
3.1	CP and OFDM symbol durations subject to 0.06 overhead	25

Chapter 1

Introduction

The amount of data handled by wireless networks is expected to be increased by well over a factor of 100. From under 3 exabytes in 2010 to over 190 exabytes by 2018, on pace to exceed 500 exabytes by 2020 [1]. In addition to the sheer volume of data, the number of devices could reach the tens or even hundreds of billions by the time 5G comes to fruition, due to many new applications beyond personal communications.

Furthermore, cumulative and incessant demands on new services and applications, in addition to the great expansion in the number of connected devices, have led to a huge data traffic explosion and appearance of different services and classifications [2]. Such services have been classified depending on use cases as follows, enhanced mobile broadband communications (eMBB), ultra-reliable and low latency communications (URLLC), and Massive machine type communications (mMTC) [3]. Thus, a strong need to boost the expected high data traffic has been recently emerged. Also, since it became obvious that the 5G has to support high data rates, applications industry and academia agreed on the necessity of new and flexible radio access technologies (RATs) [4].

In order to cope with the 5G demands, two contributions are proposed in this thesis.

Chapter 2

NOMA Multi-Numerology OFDM Systems for 5G Networks

The RAT mainly uses multiple access techniques to supply the mobile terminals with a connection to the network [5]. Designing multiple access (MA) technique is one of the most essential aspects of improving the system capacity [6]. MA techniques can be grouped into two different categories, namely, orthogonal multiple access (OMA) and non-orthogonal multiple access (NOMA) [7].

2.1 Orthogonal Multiple Access

An orthogonal scheme allows a perfect receiver to entirely separate undesirable signals from the desired signal. In other words, the signals are orthogonal to each other in orthogonal schemes [8]. Time division multiple access (TDMA), frequency division multiple access (FDMA), code division multiple access (CDMA), and orthogonal frequency-division multiple access (OFDMA) are examples of OMA schemes. Fig. 2.1 illustrates a couple of OMA schemes. Due to the scarcity of the resources, OMA cannot accommodate the extremely high capacity density requirements and new solutions have to be introduced.

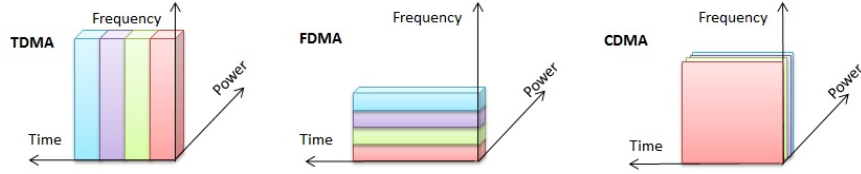


Figure 2.1: Orthogonal multiple access techniques.

2.2 Conventional Power-Domain NOMA

In contrast to OMA, NOMA allows multiple users to share the same resources, i.e., time, frequency, and code, within the same cell [9]. The current NOMA techniques can be categorized into two groups, namely, power-domain and code-domain NOMA [10]. Our work focuses on the power-domain NOMA that superposes multiple users in power domain and exploits the channel gain difference between the multiplexed users [11]. Power domain NOMA adopts multiplexing multiple users through superposition coding (SC) at the transmitter (TX). Furthermore, it uses successive interference cancellation (SIC) as a multiuser detection (MUD) technique to separate the users through power differences at the receiver (RX) side [12]. The illustration of power-domain NOMA transmission is depicted in Fig. 2.2.

The SIC is a well-known physical layer technique which basically depends on power differences for detection [13]. Briefly, SIC allows a RX to receive two or more signals at the same time. Then, the RX decodes the stronger signal, subtract it from the combined signal, and decode the weaker one from the residue.

In order to achieve the fairness in the system and provide the capability of detection at the RX side using SIC, the composed signals are assigned different power levels depending on the users' distribution. So, high power is assigned to the poor users, i.e., far users, and low power to ones whose channel conditions are good [14].

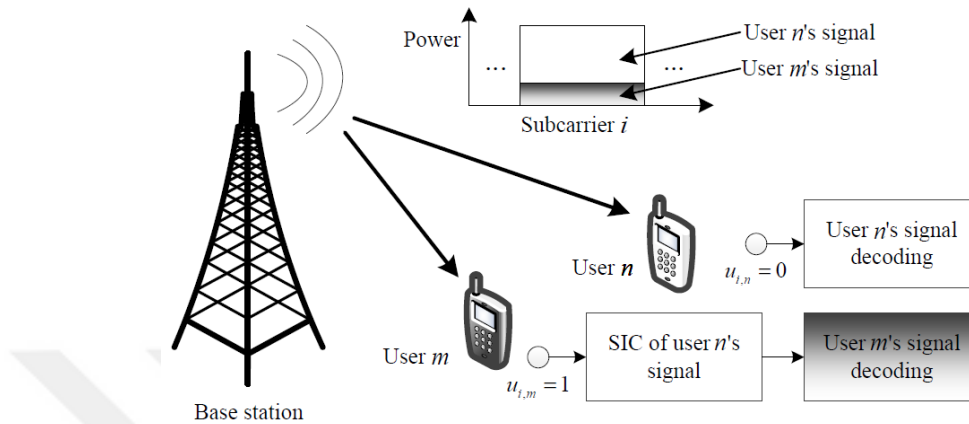


Figure 2.2: Power-domain NOMA.

2.3 Main Advantages of NOMA

- **High spectral efficiency (SE):** Consider a scenario, where a user with poor channel conditions, i.e., at the cell edge, needs to be served for fairness purposes. In OMA case, it is inevitable that one of the scarce bandwidth resources is solely occupied by this user, despite its poor channel conditions. Obviously, this has a negative effect on the spectrum efficiency and throughput of the overall system. In this situation, the use of NOMA ensures not only that the user with poor channel conditions is served but also that users with better channel conditions can concurrently utilize the same bandwidth resources as the weak user. As a result, if user fairness is a system requirement, the system throughput of NOMA can be significantly larger than that of OMA [15].
- **Fairness:** One of the key features of NOMA is that it assigns more power to the weak users and low power to the strong users. By doing so, NOMA is capable of guaranteeing an attractive trade-off between the fairness among users in terms of their throughput [16].
- **Support massive connectivity:** The future 5G network has to support the Internet of Things (IoT) functionalities. Consider a scenario where a user only needs a low data rate, e.g. IoT networks, then, the use of OMA gives the IoT node more capacity than it needs. In contrast to OMA,

NOMA is capable of serving the users by using less transmission power [17].

2.4 Numerology Concept

Numerology (NR) refers to waveform parameterization, e.g., cyclic prefix (CP), subcarrier spacing (SCS), in orthogonal frequency division multiplexing (OFDM) systems. In Third Generation Partnership Project (3GPP) discussions, it has been highlighted on NR concept where OFDM, with different parameters, is proposed as a solution to cope with 5G requirements [18]. Multiple CP and SCS families have been defined for NR concept [19]. For example, in order to decrease the sensitivity to carrier frequency offset (CFO) or phase noise, large SCSs can be used. In this work, the NR concept, i.e., different SCSs, is utilized in NOMA systems. The details are shown later.

2.5 Problem Description

It is shown that, by adopting NOMA with OFDM-based as a RAT, multiple users can be allocated on a subcarrier at the same time. However, the co-channel interference (CCI) per subcarrier increases as more users are multiplexed on the same subcarrier, which degrades the decoding capability [20]. In [15], the authors have studied users' pairing, then they concluded that NOMA outperforms OMA especially with users whose channel conditions are more distinctive, which is practically difficult to occur.

Power control/allocation has been studied in many works [16]. To guarantee the fairness among NOMA users, more power is required for users with poor channel conditions and less power for users with better channel conditions [12]. However, if the users have similar channel conditions, OMA can guarantee better fairness and conventional power domain NOMA cannot strictly guarantee the users' quality of service (QoS) targets [8], which could be critical for some

scenarios with strict fairness constraints.

We propose an OFDM based NOMA scheme. The scheme utilizes the NR concept, i.e., different SCSs, to reduce the constraints associated with the conventional NOMA schemes.

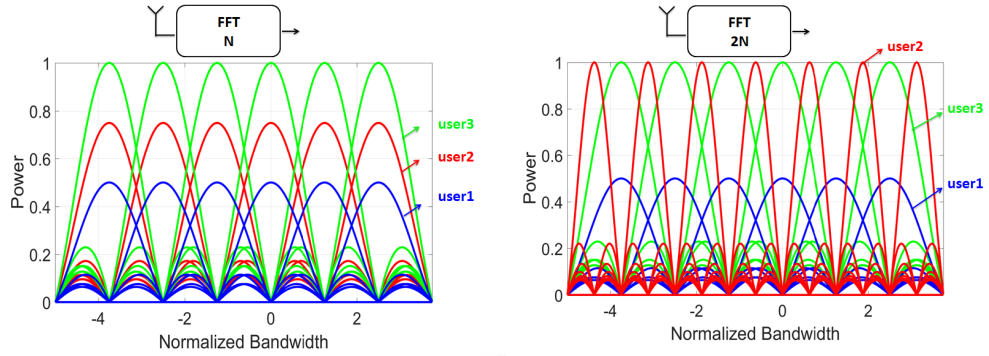
2.6 Proposed Solution

NOMA has been widely studied and is considered as a promising MA for the future 5G networks. However, degradation in the performance cannot be avoided for some specific scenarios as discussed earlier. In order to address such problems, a novel scheme is proposed. The proposed scheme basically utilizes the NR concept to reduce the constraints associated with the conventional NOMA schemes. Simply, the users utilize different SCSs, wide subcarriers and narrow subcarriers.

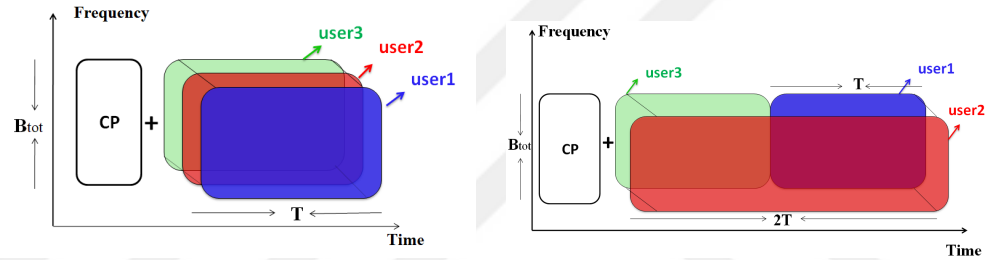
A three-user scenario is considered in this study. In the conventional scheme, the three users are supposed to share the same subcarriers as shown in Fig. 2.3(a), while in the proposed scheme, one user is assigned narrower and less frequently spaced subcarriers as illustrated in Fig. 2.3(b).

The subcarriers configuration of the proposed scheme is characterized in that, the wide subcarrier users are fully overlapped within the same wide subcarriers and make a zero crossing at the peaks of the other wide subcarriers. Furthermore, the narrow subcarriers do not impose any interference at the peaks of wide subcarriers, i.e., by avoiding the transmission on the half of narrow subcarriers. As a result, the wide subcarriers are not affected by any external interference. On the other hand, an interference is imposed by the tails of the wide subcarriers on the peaks of the narrow subcarriers.

Even though the narrow subcarriers share the bandwidth with the wide subcarriers, the detection, of wide subcarrier users, is independent of narrow subcarrier users, therefore, SIC can be used to detect the wide subcarrier users based on



(a) Carrier representation for conventional NOMA at the RX end. (b) Carrier representation for proposed NOMA at the RX end.



(c) Time representation for conventional NOMA at the TX end. (d) Time representation for proposed NOMA at the TX end.

Figure 2.3: Signals superposition in time and frequency domains.

their power differences. On the other hand, the narrow subcarriers are detected once the interference imposed by wide subcarriers is eliminated.

By assigning one of the users narrower subcarriers, we reduce the amount of CCI imposed on the wide subcarrier users. Furthermore, the interference imposed on the narrow subcarrier user can be easily canceled by eliminating the wide subcarrier signals, which enhances the bit error rate (BER) performance for each user.

The narrow subcarrier user has an extra degree of freedom (DoF) as its power level is independent of the detection process, i.e., it is not restricted to the wide subcarrier users and does not affect their detection process. In other words, the SIC process does not depend on the power level of the narrow subcarriers which grants more flexibility for power assigning. Based on that, the proposed scheme has the advantage of providing a fairer rate allocation to the users compared with

the conventional scheme especially when the channel conditions of the users are similar.

The corresponding time structure for the conventional NOMA scheme is depicted in Fig. 2.3(c). On the other hand, the proposed subcarriers configuration in Fig. 2.3(b) can be simply accomplished by composing the symbols of wide subcarrier users synchronously in the time domain, i.e., each with a length of one OFDM symbol slot. Then, the extended OFDM symbol, i.e., narrow subcarrier user, is added. However, a novel structure is adopted for the transmission. As shown in Fig. 2.3(d), the OFDM symbol slots of wide subcarrier users are orthogonally constructed and then the extended symbol of narrow subcarrier user is added. In this case, the wide subcarrier users are composed at the RX end and the proposed subcarrier configuration is obtained. In both transmission structures, the resulted signal consists of two OFDM symbol slots and the utilized resources are the same.

To achieve this purpose, the fast Fourier transform (FFT) operation, with the length of two OFDM symbol slots, is performed at the RX end. By doing this, the wide subcarrier users are multiplexed at the RX end. Extending the length of FFT window at the RX end allows us to equalize the channel using one CP [21], which is a good solution to increase the SE even with an absolute OFDMA system. More details are represented in chapter III.

2.7 Signal Configuration

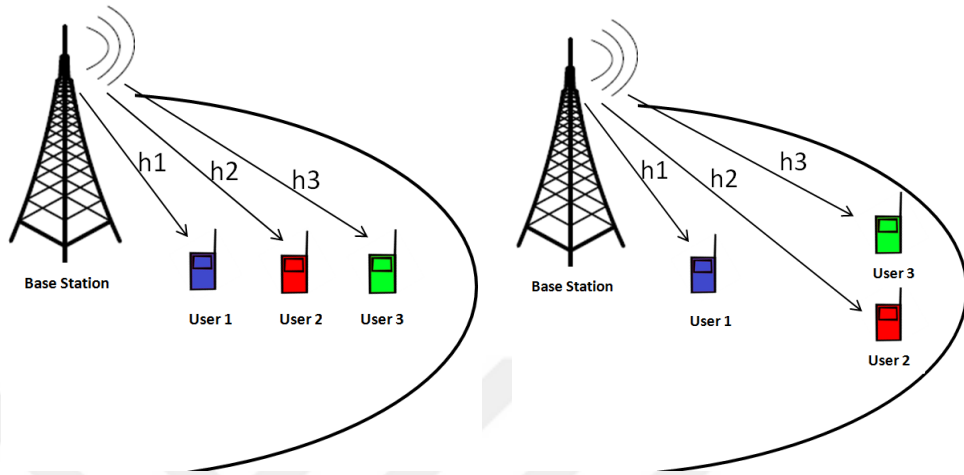
The frequency and time representations, for conventional NOMA scheme, are shown in Fig. 2.3(a) and Fig. 2.3(c) respectively. Three different power signals are multiplexed utilizing the same resources, where each signal constitutes one OFDM symbol slot, then a CP is appended. Therefore, the SE is expected to be doubled 3 times compared with OFDMA system without considering the CP redundancy.

On the other hand, in proposed NOMA, one of the users (user-2) is assigned narrower and less frequently subcarriers as illustrated in Fig. 2.3(b), which simply multiplies the symbol duration by two as depicted in Fig. 2.3(d). Since the new structure uses only T seconds out of a possible $2T$, the SE, defined as bps/Hz, is halved for the wide subcarrier users. Meanwhile, as the total energy budget is the same, the power used by wide subcarrier users is twice as before. As the SE increases logarithmically with power, this increase does not compensate for the .5 loss in the SE, thus, the overall SE improvement over OFDMA is greater than 1 but strictly less than 1.5.

As mentioned earlier, the subcarriers' configuration in Fig. 2.3(b) can be obtained if both symbols of user-1 and user-3 share the first half of user-2 symbol. However, in Fig. 2.3(d), user-1 and user-3 are constructed orthogonally at the TX. In this case, the subcarriers' configuration of the proposed scheme is accomplished at the RX end where the wide subcarrier users (user-1 and user-3) are multiplexed by adopting an extended FFT operation.

In Fig. 2.3(d), user-3 symbol is multiplexed with the first half of user-2 symbol and user-1 does the same with the second half. This can be seen from Fig. 2.3(b) as well, where user-2 has a contribution from user-1 and user-3 at the peaks. Note that, user-1 and user-3 are orthogonal with respect to each other at the TX side. However, processing them together at the RX side, i.e., by using an extended FFT window, makes them overlapping and therefore non-orthogonal. As the basic NOMA concept based on multiplexing the users at the TX utilizing the same resources, the proposed scheme can be considered as a half NOMA.

The key advantage of using larger FFT window size at RX is the capability of equalizing the channel using one CP for the whole OFDM symbols and thus increasing the SE. This property can be even used for a pure OFDMA system. For example, in the absence of user-2 in Fig. 2.3(d), the system becomes an OFDMA system. Then, if FFT operation, with the length of two OFDM symbols, is performed at the RX, the transmitted symbols are composed and one CP can be used for equalization rather than two. In our case, the composed signals are detected in power domain and user-2 is able to share the other users' resources



(a) First scenario, $|h_{1,w}| > |h_{2,w}| > |h_{3,w}|$. (b) Second scenario, $|h_{1,w}| > (|h_{2,w}| = |h_{3,w}|)$.

Figure 2.4: Two different user distribution scenarios.

without introducing any extra interference.

Note that, user-2 signal (narrow subcarriers) makes a zero crossing with the other signals (wide subcarriers) at the peaks. This can be clearly concluded from frequency domain representation. The same result is not obvious from time domain representation. Later on, it is proven mathematically that, by adopting an extended FFT window size at the RX end, the wide subcarrier users are multiplexed although they are assigned different OFDM symbol slots at the TX and the narrow subcarrier users do not affect their detection process.

2.8 Conventional NOMA Versus Proposed NOMA

To describe the features of our proposed scheme, two scenarios are considered. The first scenario appears in Fig. 2.4(a) where three downlink users have distinctive channel conditions $|h|$, while the second scenario appears in Fig. 2.4(b), where two users have similar channel conditions, i.e., two users at the cell edge and one user is close to the base station (BS).

In the case of the users whose channel conditions are similar, like the second scenario, either we assign similar power allocation (PA) to achieve the fairness, therefore, SIC cannot work properly due to its inherent nature which depends on power differences for separation, or we assign different PA which leads explicitly to unfairness distribution.

2.8.1 Conventional NOMA (CN)

If users have distinctive $|h|$ as represented in Fig. 2.4(a), under perfect channel state information (CSI) assumption at the BS, achieving the fairness can be ensured through a proper PA. Furthermore, degradation in the performance due to the number of assigned users is expected. For instance, user-3 signal has to be detected with the presence of user-2 and user-1 signals by considering them as a noise, which degrades the BER performance.

In the second scenario, user-2 and user-3 experience the same channel effect. Therefore, if the fairness is a system requirement, both users have to be assigned similar PA. However, the nature work of SIC depends on the power differences to facilitate the separation process. Thus, with similar PA, the internal interference cannot be avoided and the performance can be extremely degraded.

2.8.2 Proposed NOMA (PN)

According to the first scenario, by assigning user-2 narrow subcarriers, we reduce the interference imposed on user-1 and user-3 signals. Thus, SIC process becomes easier since it has to differentiate two signals rather than three based on their power differences. Actually, the narrow subcarrier user is selected so that the other users, i.e., wide subcarrier users, obtain more distinctive channel conditions. Besides, the PA of user-2 is determined independently which grants more flexibility for the system design.

This becomes very beneficial for the second scenario where achieving the fairness is an issue. As mentioned before, user-2 and user-3 cannot be paired as they have similar channel conditions. Nevertheless, if user-2 is assigned narrow subcarriers, user-3 and user-1 can be paired and a proper PA is determined. Naturally, the PA of user-2 is not restricted by the other users.

2.9 Conventional NOMA System Model

Conventional multicarrier downlink NOMA system is formulated by considering I downlink users around a BS as shown in Fig. 2.4. Users are distributed randomly and served by one BS and the total bandwidth B_{tot} consists of a N_{sc} number of orthogonal subcarriers in frequency domain. Transceivers are supposed to be equipped with one antenna, I users share N_{sc} OFDM subcarriers through SC.

The BS is transmitting the signal $x_{i,w}$ to the i -th user ($i = \{1, 2, \dots, I\}$) on the w -th subcarrier ($w = \{1, 2, \dots, N_{sc}\}$) with transmission power $P_{i,w}$, then, the received signal by user i on subcarrier w is given by [22] as follows

$$y_{i,w} = h_{i,w} \sum_{u=1}^I \sqrt{P_{u,w}} x_{u,w} + z_{i,w}, \quad (2.1)$$

where $z_{i,w}$ represents the additive white Gaussian noise (AWGN) for the i -th user on subcarrier w with a zero mean and $\sigma_{i,w}^2$ variance, i.e., $z_{i,w} \sim \mathcal{N}(0, \sigma_{i,w}^2)$, and $h_{i,w}$ denotes the channel gain between the BS and the received user at the w -th subcarrier including both effects of large and small scale fading. For large scale fading, path loss and shadowing are considered. Block Rayleigh is considered for small scale fading as well.

Without loss of generality, the channels are sorted as $|h_{1,w}|^2 > |h_{2,w}|^2 > \dots > |h_{i,w}|^2 > \dots > |h_{I,w}|^2 > 0$. Assuming a perfect CSI is available at the TX side, for a given subcarrier, a user who enjoys a better downlink channel quality can decode and remove the CCI from a user who has a worse downlink channel quality by employing SIC [20], thus, user i enjoys a better channel quality than user $(i + 1)$. At the i -th user, if SIC is carried out perfectly, then achieving the fairness follows

Shannon's equation [23], where the achievable rate of the i -th user for B_{tot} Hz system bandwidth at the RX side is given by

$$R_i = B_{sc} \sum_{w=1}^{N_{sc}} \log_2(1 + SINR_{i,w}), \quad \text{where} \quad (2.2)$$

$$SINR_{i,w} = \left(\frac{P_{i,w} |h_{i,w}|^2}{|h_{i,w}|^2 \sum_{u=1}^{i-1} P_{u,w} + \sigma_{i,w}^2} \right).$$

Here $SINR_{i,w}$ is the instantaneous signal-to-interference-plus-noise ratio by user i on the w -th subcarrier and $B_{sc} = B_{tot}/N_{sc}$ is the subcarrier bandwidth. Note that, if the strongest user, i.e., user-1, decodes and cancels all other users' signals successively, then, the achievable data rate is given by $R_1 = B_{sc} \sum_{w=1}^{N_{sc}} \log_2(1 + P_{1,w} |h_{1,w}|^2 / \sigma_{1,w}^2)$.

2.10 Proposed NOMA Design Analysis

This section considers the design analysis of our proposed scheme. The mathematical model of the proposed scheme is established. The time domain signal in Fig. 2.3(d) is formulated. Then, it is shown that, by adopting FFT operation with a length of two OFDM symbols at the RX side, the wide subcarrier users are composed although they are orthogonally transmitted.

Generation of wide subcarrier signals can be done using an inverse fast Fourier transform (IFFT) process with a length of N samples. On the other hand, narrow subcarrier signals can be also generated using IFFT process with a length of $M = QN$ samples, where Q is the ratio between the two different SCSs or the two different symbol lengths.

According to Fig. 2.3(b), user-1 and user-3 signals are generated using IFFT with N points, while user-2 signal utilizing IFFT with $M = 2N$ points. It is worthy to mention that, to avoid direct interference with wide subcarriers we do not use all of the narrow subcarriers for transmission. In our example, narrow-odd subcarriers are used for user-2 data transmission while narrow-even ones are filled with zeros using subcarrier mapping (SM).

An OFDM transmission symbol, of wide subcarrier user, is given by the N point complex modulation sequence

$$x_{w_a}(n) = \sqrt{P\alpha_a}IFFT(X_{w_a}) = \frac{1}{N}\sqrt{P\alpha_a}\sum_{k=0}^{N-1}X_{w_a}(k).e^{j2\pi nk/N}, \quad (2.3)$$

for $n = 0, 1, \dots, N - 1$ *and* $a = 0, 1, \dots, A$.

Where $X_{w_a}(k)$ is the complex modulated symbol of a -th user on k -th subcarrier, i.e., A is the number wide subcarrier users, α_a is the assigned PA factor to the a -th user and $\sum_{a=1}^A P\alpha_a$ is the amount of power that is specified for wide subcarrier users.

In a similar way, the OFDM transmission symbol, for narrow subcarrier user, is given by the M point complex modulation sequence

$$x_{nr_b}(m) = \sqrt{P\beta_b}IFFT(\hat{X}_b) = \frac{1}{M}\sqrt{P\beta_b}\sum_{l=0}^{M-1}\hat{X}_b(l).e^{j2\pi ml/M}, \quad (2.4)$$

for $m = 0, 1, \dots, M - 1$ *and* $b = 0, 1, \dots, B$.

$$\hat{X}_b(l) = \begin{cases} X_{nr_b}\left(\frac{l-1}{Q}\right), & l = Qk + 1, (l = 1, 3, \dots, M - 1) \\ 0, & \text{o.w.} \end{cases} \quad (2.5)$$

Where $\hat{X}_b(l)$ is the complex modulated symbol of b -th user on l -th subcarrier after SM, i.e., B is the number narrow subcarrier users, β_b is the assigned PA factor to the b -th user, $\sum_{b=1}^B P\beta_b$ is the amount of power that is specified for narrow subcarrier users, $I = A + B$ is the total number of users, and the maximum assigned power from the BS to all users is $P = \sum_{a=1}^A P\alpha_a + \sum_{b=1}^B P\beta_b$, i.e., $B = 0$ represents the conventional NOMA scheme case.

The wide subcarrier signals (x_w) are assigned different time slots to form one block xx_w with a length of M samples. Thereafter, the narrow subcarrier signals (x_{nr}) are added together forming another block xx_{nr} which is already with a length of M samples. Finally, the resultant blocks are added synchronously to produce one block s with a length of M samples for the transmission, this process can be

expressed as follows

$$s = \mathbf{X}\mathbf{X}_w + \mathbf{X}\mathbf{X}_{nr}, \quad \text{where,} \quad (2.6)$$

$$\mathbf{X}\mathbf{X}_w = [\mathbf{x}_{w_1}, \dots, \mathbf{x}_{w_A}]_{M=AN}, \quad \mathbf{X}\mathbf{X}_{nr} = \sum_{b=1}^B \mathbf{x}_{nr_b}.$$

According to the proposed scheme in Fig. 2.3, $A = 2$, $B = 1$, $M = 2N$ and $Q = 2$. So (2.6) can be written as follows

$$\mathbf{X}\mathbf{X}_w = [\mathbf{x}_{w_1}, \mathbf{x}_{w_2}]_{2N}, \quad \mathbf{X}\mathbf{X}_{nr} = [\mathbf{x}_{nr_1}]_{M=2N}. \quad (2.7)$$

By assuming $m = n + qN$, (2.4) can be represented in a block manner

$$x_{nr}(n + qN) = \frac{1}{M} \sum_{k=0}^{N-1} \sqrt{P\beta_1} X_{nr}(Qk + 1) \cdot e^{j2\pi(n+qN)(Qk+1)/M}, \quad (2.8)$$

for $n = 0, 1, \dots, N - 1$ and $q = 0, 1, \dots, Q - 1$.

Since $Q = 2$, the first half and second half of x_{nr} signal can be represented by setting q to 0 and 1 respectively

$$x_{nr}(n) = \frac{1}{M} \sum_{k=0}^{N-1} \sqrt{P\beta_1} X_{nr}(Qk + 1) \cdot e^{j2\pi n(Qk+1)/M}, \quad \text{for } q = 0$$

$$x_{nr}(n + N) = \frac{1}{M} \sum_{k=0}^{N-1} \sqrt{P\beta_1} X_{nr}(Qk + 1) \cdot e^{j2\pi(n+N)(Qk+1)/M}, \quad \text{for } q = 1 \quad (2.9)$$

$$x_{nr}(n + N) = -x_{nr}(n), \quad \text{for } n = 0, 1, \dots, N - 1.$$

Thus, the second half of the signal x_{nr} is just a reversal copy of the first half in time domain because of the odd subcarriers usage (see Appendix 5.1 for the derivation details). Based on (2.9), the transmitted signal s in (2.6) can be expressed as follows

$$s(v) = \begin{cases} x_{w_1}(v) + x_{nr_1}(v), & 0 < v < N - 1 \\ x_{w_2}(v) - x_{nr_1}(v), & N < v < 2N - 1, \end{cases} \quad (2.10)$$

where v represents the composed signal sample index ($v = \{0, 1, \dots, M - 1\}$).

After composing the signals, to avoid inter-symbol interference and enable frequency domain equalization (FDE) at the RX, a copy from the resultant tail is appended as a CP where its duration has to be larger than the maximum excess delay of the channel.

At the RX end and after removing the CP, FFT operation, with a length of $M = 2N$ points, is performed as follows

$$S(c) = \sum_{v=0}^{M-1} s(v).e^{-j2\pi vc/M} \quad \text{for } c = 0, 1, \dots, M - 1. \quad (2.11)$$

Where S are the received complex symbols after FFT operation. Afterwards, FDE takes the responsibility to get rid of channel's sparsity where single tap equalization is available. To compute the output on the even and odd subcarriers, we assume that $c = Qk + q$, then, (2.11) can be represented as

$$S(Qk + q) = \sum_{v=0}^{N-1} \left(x_{w_1}(v) + x_{nr_1}(v) \right).e^{-j2\pi v(Qk+q)/QN} + \sum_{v=N}^{2N-1} \left(x_{w_2}(v) - x_{nr_1}(v) \right).e^{-j2\pi v(Qk+q)/QN}. \quad (2.12)$$

By setting $q = 0$ and assuming $z = v - N$ for the second part of (2.12), then, the output on even subcarriers is proven to be

$$S(Qk) = \sqrt{P\alpha_1}X_{w_1}(k) + \sqrt{P\alpha_2}X_{w_2}(k), \quad \text{for } k = 0, \dots, N - 1. \quad (2.13)$$

Explicitly, (2.13) proves that, although X_{w_1} and X_{w_2} signals are constructed orthogonally at the TX, they are multiplexed by utilizing larger FFT window at the RX side (see Appendix 5.1 for the derivation details). In addition, (2.13) assures the absence of narrow subcarriers contribution to wide subcarriers, thereafter, SIC separates the wide subcarrier signals based on power differences.

Table 2.1: Simulation Parameters.

Parameter Name	Value
No. of Wide Subcarriers (N)	64
No. of Narrow Subcarriers (M)	128
Modulation Type	QPSK
Total System Bandwidth	5 MHz
Total Power	10 dBm
The First Scenario $ h_{i,w} ^2/\sigma_{i,w}^2$	20dB, 17dB, 0dB for $i = 1, 2, 3$
The Second Scenario $ h_{i,w} ^2/\sigma_{i,w}^2$	20dB, 0dB, 0dB, for $i = 1, 2, 3$

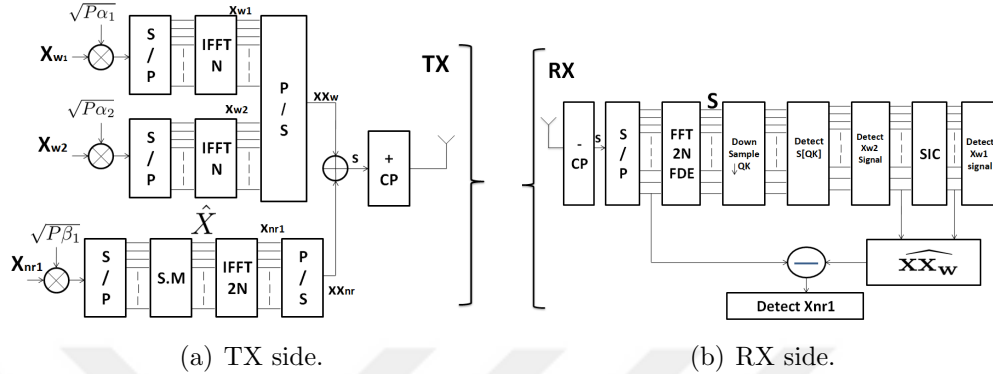


Figure 2.5: Transceiver design for proposed NOMA scheme adopting three down-link users.

User-1 and user-3 signals are constructed again, then, the reconstructed signal \widehat{xx}_w is subtracted from the received signal s with a view to detect user-2 signal. The transceiver block diagram is given in Fig. 2.5 for the proposed NOMA scheme.

2.11 Performance Evaluation

In this section, we evaluate the performance of proposed NOMA scheme through simulation. System parameters are presented in Table 2.1.

2.11.1 BER

The BER performance is supposed to be enhanced by performing proposed NOMA due to many reasons. Mainly, wide subcarrier users experience less number of interferer users. Moreover, the interference imposed on narrow subcarrier user can be eliminated by detecting and canceling wide subcarrier users and utilizing the unused narrow subcarriers. Furthermore, the narrow subcarrier user can enjoy any power level. Thus, the BER performance is enhanced significantly. Note that, the $SINR$ values are considered at the RX side after FFT process.

The $SINR_{i,w}^c$ values utilizing conventional NOMA scheme for user-1, user-2, and user-3 on subcarrier w , with successful decoding and no error propagation assumption, are given by

$$\begin{aligned} SINR_{1,w}^c &= \left(\alpha_1 P |h_{1,w}|^2 / \sigma_{1,w}^2 \right), SINR_{2,w}^c = \left(\frac{\alpha_2 P |h_{2,w}|^2}{|h_{2,w}|^2 \alpha_1 P + \sigma_{2,w}^2} \right), \\ SINR_{3,w}^c &= \left(\frac{\alpha_3 P |h_{3,w}|^2}{|h_{3,w}|^2 (\alpha_1 + \alpha_2) P + \sigma_{3,w}^2} \right). \end{aligned} \quad (2.14)$$

The $SINR_{i,w}^p$ values utilizing proposed NOMA scheme are expressed as follows

$$\begin{aligned} SINR_{1,w}^p &= \left(\alpha_1 P |h_{1,w}|^2 / \sigma_{1,w}^2 \right), SINR_{2,w}^p = \left(\beta_1 P |h_{2,w}|^2 / \sigma_{2,w}^2 \right), \\ SINR_{3,w}^p &= \left(\frac{\alpha_2 P |h_{3,w}|^2}{|h_{3,w}|^2 \alpha_1 P + \sigma_{3,w}^2} \right). \end{aligned} \quad (2.15)$$

Using the same PA for both schemes, we can notice from (2.14) and (2.15) that the first user experiences the same $SINR$ values, while a big enhancement, in $SINR$ values, is noticeable for the second and third user utilizing proposed NOMA.

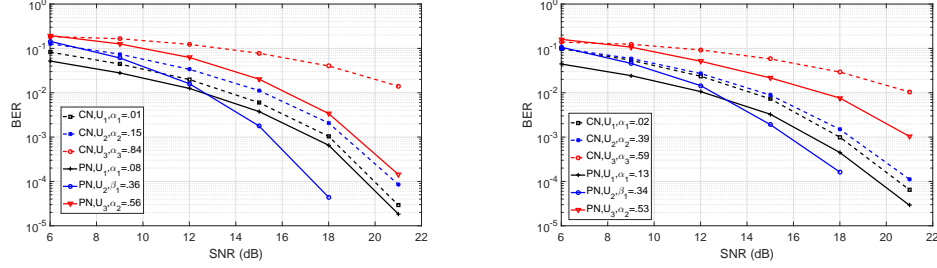
2.11.2 Fairness Factor (F)

To evaluate the fairness level for conventional and proposed NOMA we define the factor F as in [24], where F measures the equality of users' rate R for a given system and it is given by

$$F = \frac{(\sum_{i=1}^I R_i)^2}{I \sum_{i=1}^I (R_i)^2}. \quad (2.16)$$

For instance, If all users get the same amount of R , then the value F will be close to 1.

The goal of PA mechanism is to maximize the sum capacity under a fairness



(a) BER performance utilizing the optimum PA for conventional and proposed NOMA in the first scenario, $\bar{F} = 0.7$. (b) BER performance utilizing the optimum PA for conventional and proposed NOMA in the second scenario, $\bar{F} = 0.7$.

Figure 2.6: BER performance utilizing conventional and proposed NOMA.

constraint for NOMA systems. The optimization problem is formulated as

$$\begin{aligned}
 \max_{\alpha_a, \beta_b} \quad & B_{sc} \sum_{i=1}^I \sum_{w=1}^{N_{sc}} \log_2(1 + SINR_{i,w}) \\
 s.t. : \quad & \sum_{i=1}^I \sum_{w=1}^{N_{sc}} P_{i,w} \leq P \\
 & P_{i,w} \geq 0, \forall i, \forall w \\
 & F = \bar{F},
 \end{aligned} \tag{2.17}$$

where \bar{F} is the target fairness index in the network. The PA coefficients (α_a, β_b) are obtained through exhaustive search using algorithm 1 in [25].

According to the first scenario, the optimal PA coefficients utilizing conventional NOMA and proposed NOMA schemes equal to $[\alpha_1 \alpha_2 \alpha_3] = [0.01 \ 0.15 \ 0.84]$ and $[\alpha_1 \beta_2 \alpha_2] = [0.08 \ 0.36 \ 0.56]$ respectively. On the other hand, based on the second scenario, the optimal PA coefficients utilizing conventional NOMA and proposed NOMA are found to be $[\alpha_1 \alpha_2 \alpha_3] = [0.02 \ 0.39 \ 0.59]$ and $[\alpha_1 \beta_2 \alpha_2] = [0.13 \ 0.34 \ 0.53]$ respectively.

Using the optimal PA coefficients, the BER performance is evaluated. The normalized channel gains $(|h_{i,w}|^2 / \sigma_{i,w}^2)$ are set as in Table 2.1 and the fairness index \bar{F} is assumed to be 0.7. The individual BER for the first and the second scenarios are shown in Fig. 2.6(a) and Fig. 2.6(b) respectively. Depending on the optimal PAs obtained for the second scenario, the fairness level, of conventional and proposed NOMA schemes, is evaluated as depicted in Fig. 2.7. The results

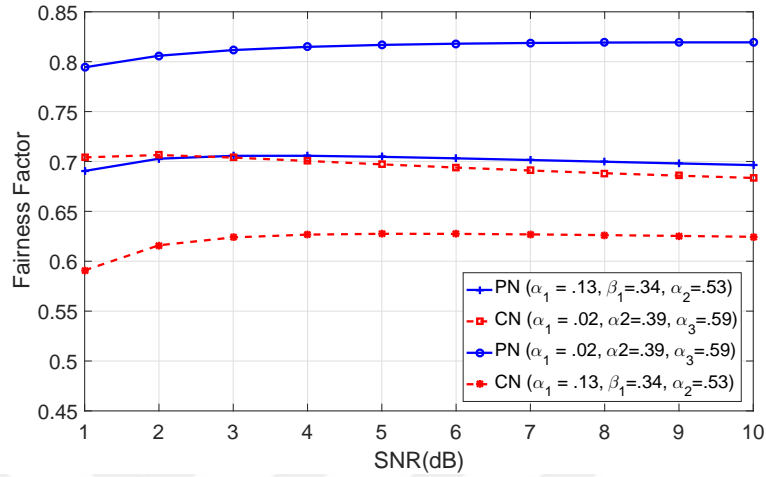


Figure 2.7: Fairness level of conventional and proposed NOMA utilizing the optimum PA for the second scenario.

show clear dominance of proposed NOMA over conventional NOMA in terms of BER and fairness level.

2.11.3 Spectral Efficiency (SE)

The spectral efficiency $\eta_i = R_i/B_{tot}$ represents the amount of the carried data over the available resources. In [26], it is proven that the conventional NOMA schemes can offer a better SE than OMA.

In conventional NOMA, the SE is expected to enhance dramatically since three users utilize the available resources, i.e., time and frequency units. Unfortunately, this comes at a price of unguaranteed QoS and loss of fairness. On the other hand, although proposed NOMA offers less SE than conventional NOMA due to additional time unit usage, i.e., two-time slots, it still provides superior SE than OMA. In particular, the superior SE in proposed NOMA arises from the capability of the narrow subcarrier user to share the available resources in addition to CP reduction between OFDM symbols.

The first scenario in Fig. 2.4(a) is considered in the evaluation of the average

SE for OMA, conventional NOMA, and proposed NOMA. For OMA, the bandwidth B_{tot} and the total power P are split equally between the assigned users. The SE performance is illustrated in Fig. 2.8. It is obvious that the SE of pro-

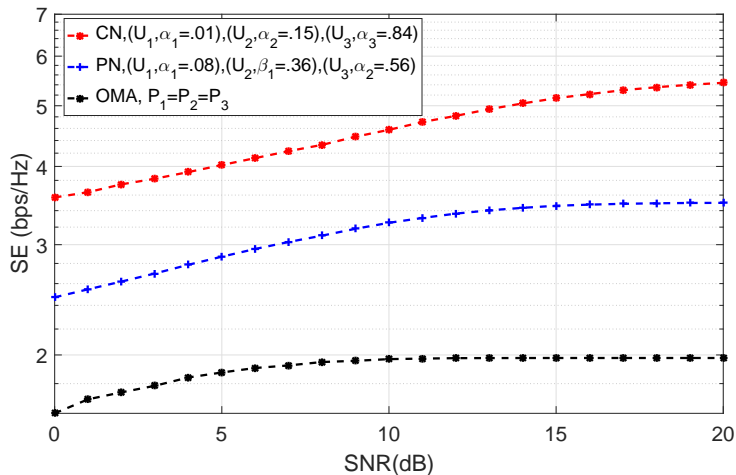


Figure 2.8: Average SE adopting conventional NOMA, proposed NOMA and OMA using the optimum PA for the first scenario.

posed NOMA is decreased compared to conventional NOMA, however, it is still more spectrally efficient than OMA.

2.12 Conclusion

In this work, some of the NOMA-OFDM system based problems have been addressed by employing NR concept cleverly. More DoF is given to one of the composed users by assigning narrower subcarriers. Based on this DoF, the constraints associated with the conventional NOMA schemes have been reduced and the BER performance has been improved too. Furthermore, the proposed method has proven its superiority in affording a fairer rate allocation to the users compared to conventional method.

A new methodology of multiplexing the users, in power domain, has been implemented by adopting a larger FFT window at the RX end. As a result,

the guard durations between OFDM symbols became unnecessary. Thus, our proposed scheme is more spectrally efficient than OMA schemes.



Chapter 3

Common Cyclic Prefix for Numerology-5G Frame Structure

Designing a waveform for wireless networks has multiple aspects that need to be taken into consideration [27]. Especially, when the emerging applications and various use cases for the 5G and beyond are considered [28].

3.1 Numerology for 5G Frame Structure

In 3GPP discussions, it has been highlighted on NR concept [29]. OFDM with different parameters is proposed as a solution to cope with 5G requirements [18]. Multiple CP and SCS families have been defined for NR concept to support the large variety of use cases [19]. For example, in order to decrease the sensitivity to CFO or phase noise, large SCSs can be used [30].

Fig. 3.1 illustrates an example of the proposed frame structure for 5G networks. Different SCSs are proposed to support different use cases. For instance, at high frequency bands, e.g., millimeter wave (mmWave), the degree of frequency shift by moving the TX or RX gets higher. To tolerate this kind of frequency

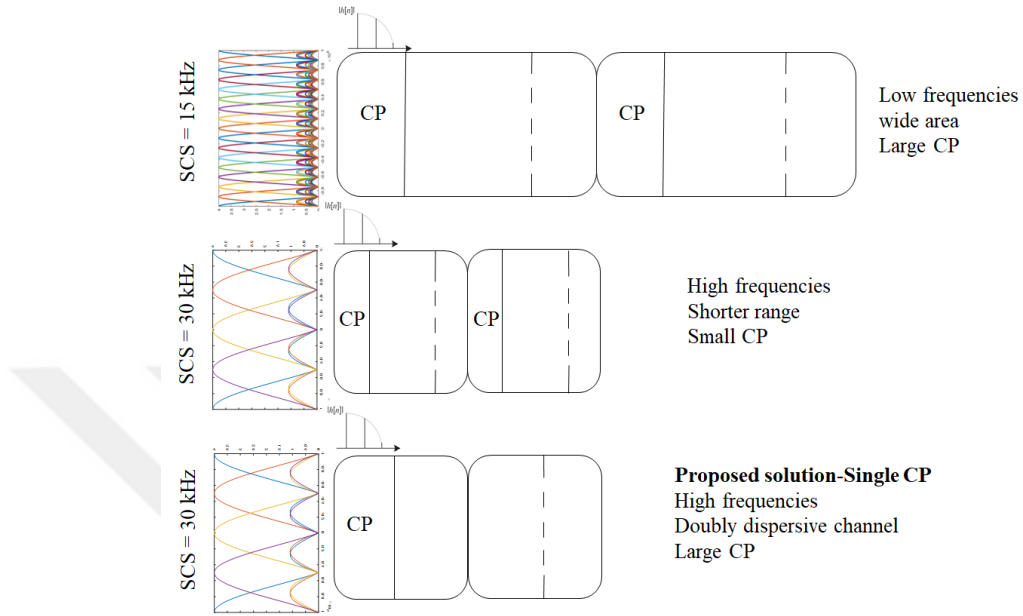


Figure 3.1: 5G-NR frame structure.

drift, the use of wider SCS becomes necessary [31]. There is another reason for wider SCS in mmWave, in implementation of beamforming, controlling the phase of the signal is critical and it is difficult to control the phase of the signal with narrow SCS [32].

3.2 Problem Description

As discussed earlier, it is preferred to use large SCSs for some specific scenarios. As a result, short OFDM symbols are obtained, i.e., due to the inverse relationship between frequency and time domains. Unfortunately, this comes at the expense of increasing the CP overhead. To push the efficiency, ultra short CPs are introduced. However, the shorted CP may not exceed the maximum excess delay of the channel which degrades the equalization performance due to the inter-symbol interference. This problem is exaggerated especially for large delay spread channels where long CPs are required. Note that, the CP overhead is defined as the CP length over the OFDM symbol length [33].

Assuming that a system is designed to tolerate 0.06 of the CP overhead, then, short CPs have to be introduced as depicted in Table 3.1. However, for doubly dispersive channels, the shortened CP may not be enough to compensate the maximum excess delay of the channel which degrades the equalization performance.

Table 3.1: CP and OFDM symbol durations subject to 0.06 overhead

SCS [kHz]	OFDM symbol [μ s]	CP [μ s]	Overhead
15	66.67	4	0.06
30	33.33	1.99	0.06
60	16.67	1	0.06
120	8.33	.499	0.06

3.3 State of Art

Note that, a common CP idea is proposed in [21] and [34] for different purposes. Also, the authors have relied on complex procedures for the detection.

3.4 Proposed Solution

We propose a novel frame structure design for 5G systems. A common CP is appended for multiple OFDM symbols at the TX side as depicted in Fig. 3.1. By doing so, the CP overhead is reduced. Thus, long CPs can be utilized even while adopting large SCSs. In other words, utilizing large SCSs becomes more applicable.

At the RX end, an enlarged FFT operation, with a length equals to the CP-removed signal, is adopted. Therefore, the FDE takes the responsibility to get rid of the channel effect where single tap equalization is available.

It is shown in chapter II that, the orthogonally transmitted symbols are constructively multiplexed if a larger FFT window size is adopted on the RX side. Based on that result, two approaches are adopted for the users' detection.

- The transmitted symbols are assigned different power levels before being multiplexed at the RX. Then, separation is done depending on power differences by utilizing SIC as a MUD technique.
- The received signal is passed through another phase. In the first phase, the CP-removed signal is undergone by the enlarged FFT operation which yields to multiplex the transmitted symbols. In the second phase, the CP-removed signal is multiplied by a diagonal matrix before implementing the extended FFT operation. The purpose of the matrix is to change the polarity of each individual symbol in order to have a specific version of the summed symbols. Finally, the phases' outputs are used for the detection.

3.5 Design Analysis

The Q OFDM symbols are generated using IFFT operation at the TX side. Each q -th OFDM transmission symbol is given by the N point complex modulation sequence

$$x_q[n] = IFFT(X_q[k], N) = \frac{1}{N} \sum_{k=0}^{N-1} X_q[k] \cdot e^{j2\pi nk/N}, \quad (3.1)$$

for $n = 0, 1, \dots, N - 1$, and $q = 0, 1, \dots, Q - 1$.

$X_q[k]$ represents the complex modulated symbol on k -th subcarrier of the q -th OFDM symbol. The generated symbols are arranged sequentially to form one block with a length of $M = QN$. Then, a CP is appended to the whole block before transmission where the CP length N_{CP} should be greater than the maximum excess delay of the channel. Here, assuming a multipath channel with L symbol-spaced paths, the CP length is set as $N_{CP} \geq L$. Fig. 3.2 shows the TX structure where two OFDM symbols are used as an example.

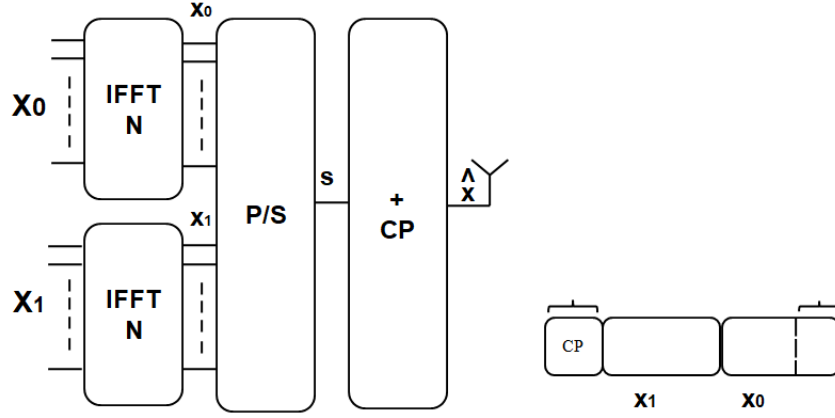


Figure 3.2: Transmitter design where $Q = 2$.

The $(QN + N_{CP})$ -dimensional transmitted signal vector is given by

$$\hat{\mathbf{x}} = \left[x_{Q-1}(N - N_{CP} + 1), \dots, x_{Q-1}(N - 1), x_0(0), \dots, x_0(N - 1), \dots, x_{Q-1}(0), \dots, x_{Q-1}(N - 1) \right]^T. \quad (3.2)$$

We assume that the channel response does not change much during the symbols plus guard interval duration. The QN -dimensional received signal vector after CP removal is given by

$$\mathbf{r} = \begin{bmatrix} h_0 & 0 & \cdots & 0 & h_L & \cdots & h_1 \\ h_1 & h_0 & \ddots & & 0 & \ddots & \vdots \\ \vdots & h_1 & \ddots & & \ddots & \ddots & h_L \\ h_L & \vdots & \ddots & \ddots & & & 0 \\ 0 & h_L & & \ddots & \ddots & & \vdots \\ \vdots & \ddots & \ddots & & \ddots & \ddots & \vdots \\ 0 & \cdots & 0 & h_L & h_1 & h_0 \end{bmatrix} \mathbf{s} + \mathbf{w}, \quad (3.3)$$

where the size of the circulant channel matrix \mathbf{h} is $[QN, QN]$. The CP-removed signal \mathbf{s} and the AWGN vector \mathbf{w} are with the size of $[QN, 1]$.

Then, an FFT operation with the length of $M = QN$, i.e., the same length of the CP-removed signal, is performed. Thus, (3.3) becomes

$$\begin{aligned} \mathbf{R} &= FFT(\mathbf{r}, QN) = \mathbf{H}\mathbf{S} + \mathbf{W} \quad \text{where,} \\ \mathbf{H} &= FFT(\mathbf{h}, QN), \mathbf{W} = FFT(\mathbf{w}, QN), \mathbf{S} = FFT(\mathbf{s}, QN). \end{aligned} \quad (3.4)$$

Assuming that the channel transfer function is known from channel estimation, channel sparsity can be compensated with (3.4) using a single-tap FDE as follows

$$\mathbf{R}^{FDE} = \frac{\mathbf{R}}{\mathbf{H}} = \mathbf{S} + \mathbf{W}^{FDE}. \quad (3.5)$$

The demodulation of each OFDM symbol can be done by converting back the frequency domain equalized signal into the time domain using an IFFT operation with the length of QN followed by Q FFT operations with the length of N for each [21]. However, this comes at the expense of increasing the computational complexity.

If the channel is perfectly equalized and no noise is introduced, then, (3.5) can be expressed as

$$\begin{aligned} \mathbf{R}^{FDE} &= \mathbf{S} = FFT(\mathbf{s}, QN) = \\ S[c] &= FFT(s[v], M) = \sum_{v=0}^{M-1} s[v].e^{-j2\pi cv/M}, \quad for\ c = 0, 1, \dots, M-1, \end{aligned} \quad (3.6)$$

where the CP-removed signal is written as

$$s[v] = \begin{cases} x_0(v), & 0 < v < N-1 \\ \cdot & \cdot \\ \cdot & \cdot \\ x_{Q-1}(v), & M-N+1 < v < M-1. \end{cases} \quad (3.7)$$

By letting $c = Qk + q$, (3.6) can be shown in an interleaved manner as

$$\begin{aligned} S[Qk + q] &= \sum_{v=0}^{N-1} x_0(v).e^{-j2\pi v(Qk+q)/QN} + \sum_{v=N}^{2N-1} x_1(v).e^{-j2\pi v(Qk+q)/QN} + \dots + \\ &\sum_{v=QN-N}^{QN-1} x_{Q-1}(v).e^{-j2\pi v(Qk+q)/QN}, \quad for\ k = 0, 1, \dots, N-1, \text{ and } q = 0, 1, \dots, Q-1. \end{aligned} \quad (3.8)$$

Setting $q = 0$ gives the output on $Qk = 0, Q, 2Q, \dots, Q(N-1)$ subcarriers

$$S[Qk] = X_0[k] + X_1[k] + \dots + X_{Q-1}[k], \quad for\ k = 0, 1, \dots, N-1. \quad (3.9)$$

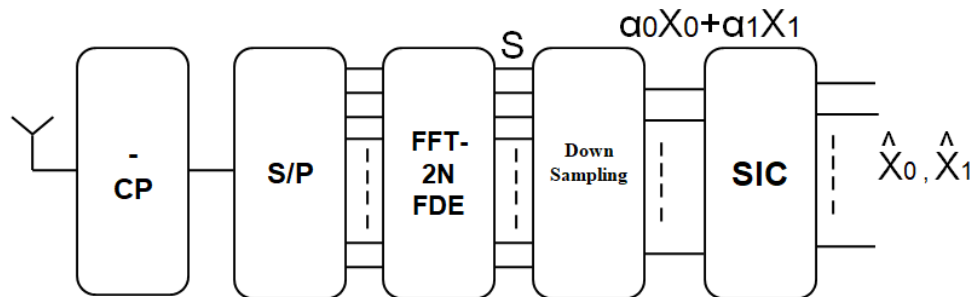


Figure 3.3: Receiver design adopting the first approach where $Q = 2$.

Clearly, (3.9) indicates that the orthogonally transmitted OFDM symbols are multiplexed on Qk subcarriers by adopting an extended FFT operation at the RX side. Note that, such the result is proven in chapter II without considering the formation of the channel.

3.6 Detection Approaches

Based on (3.9), two approaches are adopted for the detection.

3.6.1 First Approach

By assigning the transmitted symbols different power factors, i.e., $\alpha_0, \dots, \alpha_{Q-1}$, detection is performed in the power domain using SIC as a MUD technique. Note that, we do not call this approach NOMA since the symbols are composed at the RX due to the enlarged size of FFT process, while in NOMA, the symbols are composed intentionally at the TX [12]. The RX design using the first approach is depicted in Fig. 3.3 where two OFDM symbols ($Q = 2$) are considered as an example.

3.6.2 Second Approach

In the first approach and after FDE, the resultant vector, with a length of M samples, is downsampled to obtain the multiplexed symbols on Qk subcarriers for the detection. The main idea behind the second approach is to exploit the output on the other subcarriers for the detection, i.e., rather than Qk subcarriers. The second approach is studied for the case where one CP is used for every two symbols ($Q = 2$). Thus, as shown in (3.9), the output of Qk subcarriers is

$$S[2k] = X_0[k] + X_1[k] \quad \text{for } k = 0, 1, \dots, N - 1. \quad (3.10)$$

And according to (3.8), the output on $[Qk + 1]$ subcarriers is equal to

$$S[2k + 1] = \left(\sum_{v=0}^{N-1} \left(x_0(v) \cdot e^{-j2\pi vk/N} - x_1(v + N) \cdot e^{-j2\pi vk/N} \right) \cdot e^{-j\pi v/N} \right). \quad (3.11)$$

In the above equation, if the last term ($e^{-j\pi v/N}$) is forced to be one, the transmitted symbols are subtracted rather than added (see Appendix 5.1 for the derivation details). In order to compensate the terms ($e^{-j\pi v/N} = e^{-j\pi 0/N}, e^{-j\pi 1/N}, \dots, e^{-j\pi(N-1)/N}$), their conjugates are multiplied by the samples of each individual OFDM symbol of the CP-removed signal.

The term ($e^{-j\pi v/N}$) is analogous to the CFO formula. Indeed, an intentional offset is created in order to change the polarity of the symbols. Therefore, the symbols are subtracted rather than multiplexed due to the extended FFT operation. Thus, two versions of the received data can be obtained, i.e., the summed and subtracted versions. Based on that, the transmitted symbols ($X_0[k]$ and $X_1[k]$) can be easily detected.

According to the second approach, the CP-removed signal, with the length of $2N$, is multiplied by a diagonal matrix \mathbf{a} as follows

$$\tilde{\mathbf{r}} = \mathbf{a}(\mathbf{h}\mathbf{s} + \mathbf{w}), \quad \text{where } \mathbf{a} = \text{diag}(e^{+j\pi 0/N}, \dots, e^{+j\pi(N-1)/N}, e^{+j\pi 0/N}, \dots, e^{+j\pi(N-1)/N}). \quad (3.12)$$

Matrix \mathbf{a} is defined as $2N \times 2N$ matrix. Thereafter, FFT operation with $2N$ length is applied

$$\tilde{\mathbf{R}} = FFT(\tilde{\mathbf{r}}, 2N) = \tilde{\mathbf{H}}\mathbf{S} + \tilde{\mathbf{W}}. \quad (3.13)$$

Note that, the matrix \mathbf{a} is similar to the CFO matrix. This matrix can degrade the performance of FDE since the cyclicity of the channel matrix is lost [35]. Thus, $\tilde{\mathbf{H}}$ and $\tilde{\mathbf{W}}$ represent the frequency response of the channel and the noise respectively including the effect of matrix \mathbf{a} . The length of FFT here is $2N$ points.

The equalized signal can be obtained as follows

$$\tilde{\mathbf{R}}^{FDE} = \frac{\tilde{\mathbf{R}}}{\tilde{\mathbf{H}}} = \tilde{\mathbf{S}} + \tilde{\mathbf{W}}^{FDE}, \quad (3.14)$$

in this context, $\tilde{\mathbf{S}}$ represents the subtracted version of the transmitted symbols including residual components due to the degradation in FDE performance. If this degradation is ignored, i.e., $\tilde{\mathbf{H}} = \mathbf{H}$, and no noise is introduced then

$$\begin{aligned} \tilde{\mathbf{R}}^{FDE} &= FFT(\mathbf{as}, 2N) = \\ S[2k+1] &= X_0[k] - X_1[k] \quad \text{for } k = 0, 1, \dots, N-1. \end{aligned} \quad (3.15)$$

The vector representations of (3.10) and (3.15) are given by $\mathbf{C1}$ and $\mathbf{C2}$ respectively

$$\begin{aligned} \mathbf{C1} &= [(X_0(0) + X_1(0)), (X_0(1) + X_1(1)) \dots, (X_0(N-1) + X_1(N-1))]^T. \\ \mathbf{C2} &= [(X_0(0) - X_1(0)), (X_0(1) - X_1(1)) \dots, (X_0(N-1) - X_1(N-1))]^T. \end{aligned} \quad (3.16)$$

Clearly, Both $\mathbf{C1}$ and $\mathbf{C2}$ can be used for the detection process. The detected symbols $\hat{\mathbf{X}}_0$ and $\hat{\mathbf{X}}_1$ are given in the vector form as

$$\hat{\mathbf{X}}_0 = \frac{1}{2}(\mathbf{C1} + \mathbf{C2}), \quad \hat{\mathbf{X}}_1 = \frac{1}{2}(\mathbf{C1} - \mathbf{C2}). \quad (3.17)$$

The transceiver design utilizing the second approach is depicted in Fig. 3.4.

It is worthy to mention that, the degradation in FDE performance in the second approach can be ignored if it is relatively small. As the FDE is perfectly applicable in the first phase of the second approach, the degradation of FDE, due to the second phase, is halved. Thus, it is relatively small.

3.7 Performance Evaluation

In 3GPP discussions [19], the CP overhead is calculated during one sub-frame as the ratio between the time that is spent on the CP and the OFDM symbol. For

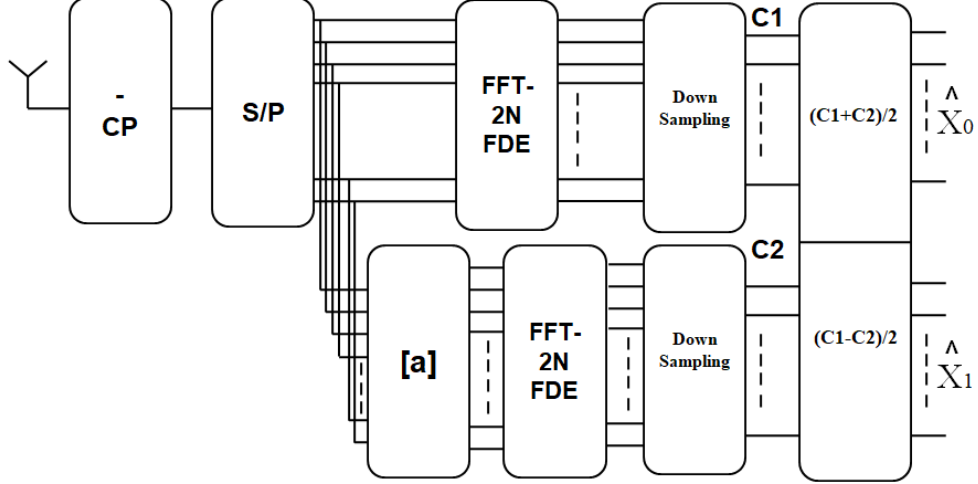


Figure 3.4: Receiver design adopting the second approach where $Q = 2$.

5G-NR frame structure, multiple SCS are adopted. According to Fig. 3.1, for the case where the SCS = 15kHz and the CP length is set to be 10 μ s, then, the CP overhead is 0.15. On the other hand, for the case where the SCS = 30kHz has to be used, and assuming that the channel shows large delay so the CP cannot be shortened, then, the CP overhead will be 0.3. In the proposed scheme, one CP can be utilized for two OFDM symbols which creates 0.15 as CP overhead. Thus, adopting larger SCSs becomes more applicable.

The SE performance is evaluated during one sub-frame as depicted in Fig. 3.5. The 4-QAM modulation is used in this simulation in addition to the aforementioned parameters of the previous example. Due to the first approach, the SIC decodes the high power signal by considering the low power signals as a noise which degrades the SE performance at low SNR values. However, the optimal SE is achievable at high SNR values. The $Q = 2$ and $Q = 3$ (one CP every 3 OFDM symbols) cases are considered in the simulation. The PAs are set as $(\alpha_1 = .7, \alpha_2 = .3)$ and $(\alpha_1 = .6, \alpha_2 = .3, \alpha_3 = .1)$ for $Q = 2$ and $Q = 3$ cases respectively.

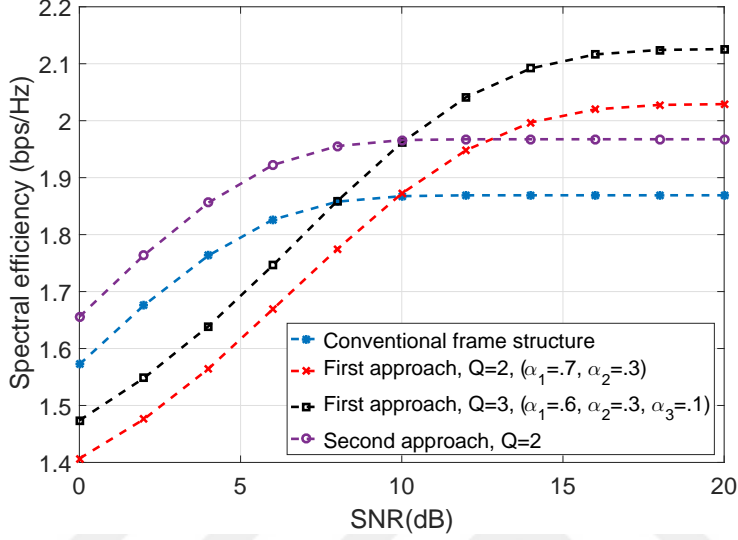


Figure 3.5: The SE performance over multipath channel, SCS = 15kHz.

The SE performance utilizing the second approach is higher than the conventional structure case for all SNR values. However, due to the imperfection of FDE, it is slightly smaller than the first approach situation at high SNR. The $Q = 2$ case is considered in the simulation utilizing the second approach.

The symbol error rates (SER) utilizing the proposed approaches are also simulated. The gain in SE is exploited to reduce the effect of CFO by enlarging the SCS. The CFO is set to .03 and the SER is evaluated as represented in Fig. 3.6.

The SE can be increased further depending on Q value. Based on the first approach, the SIC has to separate Q signals depending on the power differences. In the second approach, Q phases are needed. In each phase, the symbols are adjusted to get a specific form, then, the outputs of the phases are used to obtain the transmitted symbols.

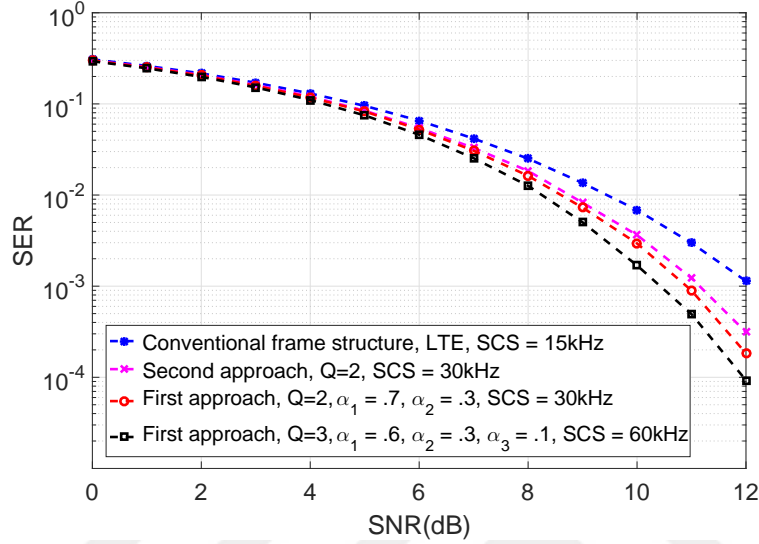


Figure 3.6: The SER performance over multipath channel where the normalized CFO = .03.

3.8 Conclusion

In this chapter, a common CP idea is proposed for the NR-5G frame structure. A single CP is appended to multiple OFDM symbols. So, the overhead associated with the frequent usage of the CP is reduced. As a result, longer CP can be used which makes the signal more tolerable to fading channel. Such the design is beneficial when large SCSs or short OFDM symbols are needed.

It is shown mathematically that, the orthogonally transmitted symbols are multiplexed due to the enlarged FFT window at the RX side. Based on that, two approaches are adopted for the detection.

Chapter 4

Future Work

In this thesis, two major contributions are made to cope with the 5G requirements. In chapter II, the NR concept is adopted in order to address the common problems associated with conventional NOMA schemes. One user is assigned narrow subcarriers which grants more flexibility to SIC process and power assigning. The proposed scheme proves its superiority not only in terms of lower BER rates but also advantageous for achieving better fairness to the whole system.

One of the attractive topics, which has to be considered in the future, is the effect of imperfect CSI at the TX side adopting the proposed NOMA scheme. Here, the resource allocation has relied on the assumption of perfect CSI at TX which is difficult to obtain in practice. In contrast to the case of perfect CSI, the capacity gain is supposed to be reduced in conventional NOMA systems as shown in many works due to

- The channels have to be estimated in advance by feeding back the BS from each receiving terminal. Clearly, this process burdens the system and increases the probability of error.
- The nature work of SIC depends on decoding the signals successively. Thus, due to the imperfect CSI, error propagation is created.

One of the good points about the proposed NOMA scheme is the independence of narrow subcarriers user from the successive decoding process. Such the user can be chosen to reduce the effect of imperfect CSI. Note that, the channel of narrow subcarriers user has not to be estimated in necessary. Therefore, we think that the proposed scheme provides better performance in terms of the sensitivity to CSI.

In this works, two kinds of SCSs are utilized together. We think that more NRs can peacefully coexist and a novel transceiver design may be founded. The importance of this work is emerging from the necessity of utilizing different NRs for different use cases which is a key requirement for 5G networks. Such the ideas are going to be considered in the future.

In chapter III, a novel transceiver design is established. Such the design aims to reduce the required CPs in OFDM systems and thus increasing the SE. Based on that, the usage of large SCSs can be adopted without introducing any overhead. It is proven mathematically that, the orthogonally OFDM-transmitted symbols are constructively multiplexed if larger FFT window size is applied at the RX end. Two detection approaches are established based on this result. Therefore, one CP can be appended multiple OFDM symbols.

A common CP idea can be further exploited. In this work, a single CP is utilized for the same NR. We think that a common CP can be used for different NRs rather than a single one. Such the idea can be adopted for the frame structure of 5G and beyond. This study will be considered in the future as well.

Chapter 5

Appendix

5.1 Appendix A: Detailed Derivations of Mathematical Equations

Here we will give the detailed derivation of (2.9), (2.13) and (3.11).

For the case where $Q = 2$ and $M = QN$, (2.8) can be written as

$$\begin{aligned}x_{\text{nr}}(n) &= \frac{1}{M} \sum_{k=0}^{N-1} \sqrt{P\beta_1} X_{\text{nr}}(Qk + 1) \cdot e^{j2\pi n(Qk+1)/M}, \quad \text{for } q = 0. \\x_{\text{nr}}(n + N) &= \frac{1}{M} \sum_{k=0}^{N-1} \sqrt{P\beta_1} X_{\text{nr}}(Qk + 1) \cdot e^{j2\pi(n+N)(Qk+1)/M} = x_{\text{nr}}(n) \cdot e^{(j2\pi N(Qk+1)/QN)} \\x_{\text{nr}}(n + N) &= x_{\text{nr}}(n) \cdot e^{j\pi} = -x_{\text{nr}}(n), \quad \text{for } q = 1, \text{ and } n = 0, \dots, N - 1.\end{aligned}\tag{5.1}$$

Such the result represents the fact that the first half of the signal x_{nr} is a reversal copy of the second half in time domain due to the odd subcarriers usage.

For the case where $q = 0$ in (2.12), the output on Qk subcarriers can be

obtained

$$S(Qk) = \sum_{v=0}^{N-1} \left(x_{w_1}(v) + x_{nr_1}(v) \right) \cdot e^{-j2\pi v(Qk)/QN} + \sum_{v=N}^{2N-1} \left(x_{w_2}(v) - x_{nr_1}(v) \right) \cdot e^{-j2\pi v(Qk)/QN}. \quad (5.2)$$

Letting $z = v - N$ for the second part of (5.2) yields to

$$\begin{aligned} S(Qk) &= \sum_{v=0}^{N-1} \left(x_{w_1}(v) + x_{nr_1}(v) \right) \cdot e^{-j2\pi vk/N} + \sum_{z=0}^{N-1} \left(x_{w_2}(z+N) - x_{nr_1}(z+N) \right) \cdot e^{-j2\pi(z+N)k/N} \\ &= \sum_{v=0}^{N-1} \left(x_{w_1}(v) + x_{nr_1}(v) \right) \cdot e^{-j2\pi vk/N} + \sum_{z=0}^{N-1} \left(x_{w_2}(z+N) - x_{nr_1}(z+N) \right) \cdot e^{-j2\pi zk/N} \\ &= \sum_{v=0}^{N-1} \left(x_{w_1}(v) + x_{w_2}(v) \right) \cdot e^{-j2\pi vk/N} = \sqrt{P\alpha_1} X_{w_1}(k) + \sqrt{P\alpha_2} X_{w_2}(k). \end{aligned} \quad (5.3)$$

Such the result represents the fact that the orthogonally transmitted symbols are multiplexed due to the enlarged FFT window.

Based on (3.8), for $Q = 2$ and $q = 1$ we get

$$\begin{aligned} S[2k+1] &= \sum_{v=0}^{N-1} x_0(v) \cdot e^{-j\pi v(2k+1)/N} + \sum_{v=N}^{2N-1} x_1(v) \cdot e^{-j\pi v(2k+1)/N} \\ S[2k+1] &= \sum_{v=0}^{N-1} x_0(v) \cdot e^{-j2\pi vk/N} \cdot e^{-j\pi v/N} + \sum_{v=N}^{2N-1} x_1(v) \cdot e^{-j2\pi vk/N} \cdot e^{-j\pi v/N} \end{aligned} \quad (5.4)$$

Letting $z = v - N$ for the second part of (5.4) yields to

$$\begin{aligned} S[2k+1] &= \sum_{v=0}^{N-1} x_0(v) \cdot e^{-j2\pi vk/N} \cdot e^{-j\pi v/N} + \sum_{z=0}^{N-1} x_1(v) \cdot e^{-j2\pi(z+N)k/N} \cdot e^{-j\pi(z+N)/N} \\ S[2k+1] &= \sum_{v=0}^{N-1} x_0(v) \cdot e^{-j2\pi vk/N} \cdot e^{-j\pi v/N} + \sum_{z=0}^{N-1} x_1(v) \cdot e^{-j2\pi zk/N} \cdot e^{-j\pi z/N} \cdot e^{-j\pi} \\ S[2k+1] &= \sum_{v=0}^{N-1} \left(x_0(v) - x_1(v) \right) \cdot e^{-j2\pi vk/N} \cdot e^{-j\pi v/N}. \end{aligned} \quad (5.5)$$

Bibliography

- [1] M. S. Corson, R. Laroia, J. Li, V. Park, T. Richardson, and G. Tsirtsis, “Toward Proximity-Aware Internetworking,” *IEEE Wireless Communications*, vol. 17, pp. 26–33, December 2010.
- [2] U. L. Rohde, A. K. Poddar, I. Eisele, and E. Rubiola, “Next Generation 5G Radio Communication NW,” in *2017 Joint Conference of the European Frequency and Time Forum and IEEE International Frequency Control Symposium (EFTF/IFC)*, pp. 113–116, July 2017.
- [3] X. Meng, J. Li, D. Zhou, and D. Yang, “5G Technology Requirements and Related Test Environments for Evaluation,” *China Communications*, vol. 13, pp. 42–51, N 2016.
- [4] J. G. Andrews, S. Buzzi, W. Choi, S. V. Hanly, A. Lozano, A. C. K. Soong, and J. C. Zhang, “What Will 5G Be?,” *IEEE Journal on Selected Areas in Communications*, vol. 32, pp. 1065–1082, June 2014.
- [5] Z. Ding, X. Lei, G. K. Karagiannidis, R. Schober, J. Yuan, and V. K. Bhargava, “A Survey on Non-Orthogonal Multiple Access for 5G Networks: Research Challenges and Future Trends,” *CoRR*, vol. abs/1706.05347, 2017.
- [6] M. S. Iacobucci and M. G. D. Benedetto, “Multiple Access Design for Impulse Radio Communication Systems,” in *2002 IEEE International Conference on Communications. Conference Proceedings. ICC 2002 (Cat. No.02CH37333)*, vol. 2, pp. 817–820 vol.2, 2002.

- [7] P. Wang, J. Xiao, and L. P, “Comparison of Orthogonal and Non-Orthogonal Approaches to Future Wireless Cellular Systems,” *IEEE Vehicular Technology Magazine*, vol. 1, pp. 4–11, Sept 2006.
- [8] Z. Ding, X. Lei, G. K. Karagiannidis, R. Schober, J. Yuan, and V. K. Bhargava, “A Survey on Non-Orthogonal Multiple Access for 5G Networks: Research Challenges and Future Trends,” *IEEE Journal on Selected Areas in Communications*, vol. 35, pp. 2181–2195, Oct 2017.
- [9] Y. Wang, B. Ren, S. Sun, S. Kang, and X. Yue, “Analysis of Non-Orthogonal Multiple Access for 5G,” *China Communications*, vol. 13, pp. 52–66, N 2016.
- [10] L. Dai, B. Wang, Y. Yuan, S. Han, C. I. I, and Z. Wang, “Non-Orthogonal Multiple Access for 5G: Solutions, Challenges, Opportunities, and Future Research Trends,” *IEEE Communications Magazine*, vol. 53, pp. 74–81, September 2015.
- [11] Z. Ding, Z. Zhao, M. Peng, and H. V. Poor, “On the Spectral Efficiency and Security Enhancements of NOMA Assisted Multicast-Unicast Streaming,” *IEEE Transactions on Communications*, vol. 65, pp. 3151–3163, July 2017.
- [12] S. M. R. Islam, N. Avazov, O. A. Dobre, and K. s. Kwak, “Power-Domain Non-Orthogonal Multiple Access (NOMA) in 5G Systems: Potentials and Challenges,” *IEEE Communications Surveys Tutorials*, vol. 19, pp. 721–742, Secondquarter 2017.
- [13] S. Sen, N. Santhapuri, R. R. Choudhury, and S. Nelakuditi, “Successive Interference Cancellation: A Back-of-The-Envelope Perspective,” in *Proceedings of the 9th ACM SIGCOMM Workshop on Hot Topics in Networks, Hotnets-IX*, (New York, NY, USA), pp. 17:1–17:6, ACM, 2010.
- [14] A. Benjebbour, Y. Saito, Y. Kishiyama, A. Li, A. Harada, and T. Nakamura, “Concept and Practical Considerations of Non-Orthogonal Multiple Access (NOMA) for Future Radio Access,” in *2013 International Symposium on Intelligent Signal Processing and Communication Systems*, pp. 770–774, Nov 2013.

- [15] Z. Ding, P. Fan, and H. V. Poor, “Impact of User Pairing on 5G Nonorthogonal Multiple-Access Downlink Transmissions,” *IEEE Transactions on Vehicular Technology*, vol. 65, pp. 6010–6023, Aug 2016.
- [16] S. Timotheou and I. Krikidis, “Fairness for Non-Orthogonal Multiple Access in 5G Systems,” *IEEE Signal Processing Letters*, vol. 22, pp. 1647–1651, Oct 2015.
- [17] Q. Wu, W. Chen, D. W. K. Ng, and R. Schober, “Spectral and Energy Efficient Wireless Powered IoT Networks: NOMA or TDMA?,” *CoRR*, vol. abs/1801.09109, 2018.
- [18] A. A. Zaidi, R. Baldemair, H. Tullberg, H. BJORKEGREN, L. Sundstrom, J. Medbo, C. Kilinc, and I. D. Silva, “Waveform and Numerology to Support 5G Services and Requirements,” *IEEE Communications Magazine*, vol. 54, pp. 90–98, November 2016.
- [19] R1-1608962, “About The Support of Multiple CP Families for NR,” ZTE, RAN1#86b, Lisbon, Portugal, 10th – 14th October 2016.
- [20] Y. Sun, D. W. K. Ng, Z. Ding, and R. Schober, “Optimal Joint Power and Subcarrier Allocation for Full-Duplex Multicarrier Non-Orthogonal Multiple Access Systems,” *IEEE Transactions on Communications*, vol. 65, pp. 1077–1091, March 2017.
- [21] X. Wang, Y. Wu, J. Y. Chouinard, and H.-C. Wu, “On the Design and Performance Analysis of Multisymbol Encapsulated OFDM Systems,” *IEEE Transactions on Vehicular Technology*, vol. 55, pp. 990–1002, May 2006.
- [22] Z. Wei, D. W. K. Ng, J. Yuan, and H. M. Wang, “Optimal Resource Allocation for Power-Efficient MC-NOMA With Imperfect Channel State Information,” *IEEE Transactions on Communications*, vol. 65, pp. 3944–3961, Sept 2017.
- [23] C. E. Shannon, “Communication in The Presence of Noise,” *Proceedings of the IRE*, vol. 37, pp. 10–21, Jan 1949.

- [24] R. K. Jain, D. M. W. Chiu, and W. R. Hawe, *A Quantitative Measure of Fairness and Discrimination for Resource Allocation in Shared Computer System*, vol. 38, pp. 20–21. Hudson, MA: Eastern Research Laboratory, Digital Equipment Corporation, 1984.
- [25] T. Manglayev, R. C. Kizilirmak, and Y. H. Kho, “Optimum Power Allocation for Non-Orthogonal Multiple Access (NOMA),” in *2016 IEEE 10th International Conference on Application of Information and Communication Technologies (AICT)*, pp. 1–4, Oct 2016.
- [26] P. Sedtheetorn and T. Chulajata, “Spectral Efficiency Evaluation for Non-Orthogonal Multiple Access in Rayleigh Fading,” in *2016 18th International Conference on Advanced Communication Technology (ICACT)*, pp. 747–750, Jan 2016.
- [27] Z. E. Ankarali, B. Pekz, and H. Arslan, “Flexible Radio Access Beyond 5G: A Future Projection on Waveform, Numerology, and Frame Design Principles,” *IEEE Access*, vol. 5, pp. 18295–18309, 2017.
- [28] M. Elkourdi, B. Pekz, E. Gvenkaya, and H. Arslan, “Waveform Design Principles for 5G and Beyond,” in *2016 IEEE 17th Annual Wireless and Microwave Technology Conference (WAMICON)*, pp. 1–6, April 2016.
- [29] A. A. Zaidi, R. Baldemair, H. Tullberg, H. BJORKEGREN, L. Sundstrom, J. Medbo, C. Kilinc, and I. D. Silva, “Waveform and Numerology to Support 5G Services and Requirements,” *IEEE Communications Magazine*, vol. 54, pp. 90–98, November 2016.
- [30] Y. Cai, Z. Qin, F. Cui, G. Y. Li, and J. A. McCann, “Modulation and Multiple Access for 5G Networks,” *CoRR*, vol. abs/1702.07673, 2017.
- [31] L. Rugini and P. Banelli, “BER of OFDM Systems Impaired by Carrier Frequency Offset in Multipath Fading Channels,” *IEEE Transactions on Wireless Communications*, vol. 4, pp. 2279–2288, Sept 2005.
- [32] J. Jeon, “NR Wide Bandwidth Operations,” *IEEE Communications Magazine*, vol. 56, pp. 42–46, MARCH 2018.

- [33] N. Kim, J. Ahn, O. S. Shin, and K. B. Lee, "Precoding Design for Cyclic Prefix Overhead Reduction in a MISO-OFDM System," *IEEE Wireless Communications Letters*, vol. 6, pp. 578–581, Oct 2017.
- [34] J. Lorca, "Cyclic Prefix Overhead Reduction for Low-Latency Wireless Communications in OFDM," in *2015 IEEE 81st Vehicular Technology Conference (VTC Spring)*, pp. 1–5, May 2015.
- [35] K. Kambara, H. Nishimoto, T. Nishimura, T. Ohgane, and Y. Ogawa, "Subblock Processing in MMSE-FDE Under Fast Fading Environments," *IEEE Journal on Selected Areas in Communications*, vol. 26, pp. 359–365, February 2008.

NOMA-MULTI NUMEROLOGY AND GUARD REDUCTION METHODS FOR OFDM SYSTEMS

ORIGINALITY REPORT

13%

SIMILARITY INDEX

8%

INTERNET SOURCES

10%

PUBLICATIONS

4%

STUDENT PAPERS

PRIMARY SOURCES

- | | | |
|---|---|-----|
| 1 | Submitted to Nashville State Community College
Student Paper | 1% |
| 2 | Submitted to Middle East Technical University
Student Paper | 1% |
| 3 | Yan Sun, Derrick Wing Kwan Ng, Zhiguo Ding, Robert Schober. "Optimal Joint Power and Subcarrier Allocation for MC-NOMA Systems", 2016 IEEE Global Communications Conference (GLOBECOM), 2016
Publication | 1% |
| 4 | scholarworks.uaeu.ac.ae
Internet Source | 1% |
| 5 | tel.archives-ouvertes.fr
Internet Source | <1% |
| 6 | www.intechopen.com
Internet Source | <1% |
| 7 | Submitted to Higher Education Commission | |